Modeling Galaxy Color Variations for Cosmological Simulations

Sam Dallas

Thesis Advisor: Professor Ian Dell'antonio

A senior thesis for Brown's Astrophysics Sc.B. degree.

May 2016

1. Abstract

This project models spectral flux density in three filters for real galaxies as a linear combination of two model spectra. Test galaxy images in the F105W, F125W and F160W filters are pulled from the HST infrared cameras in the STSCI database. For each test galaxy, model spectra from similarly redshifted galaxies are identified. Backgrounds are subtracted from the test galaxies, and a fitting algorithm is run. Each pixel in each filter of the galaxy is fitted as a linear combination of the model spectral flux density in that filter. Pixels are fitted independently of each other, but each pixel has the same coefficients for every filter. These coefficients can be used to accurately recreate galaxy images as a linear combination of the model spectra. They can be used in combination with PhoSim and image shearing algorithms to create realistic test data for gravitational lensing detection algorithms.

2. Background

In 1915, Einstein proposed his new theory of general relativity. He suggested that physicists think of space and time as a 4-D space. Objects that have mass stretch this surface, which affects the motion of other objects around them. Einstein's new theory of general relativity fit with the accepted theory of Newtonian gravity, but also explained a few stubborn gravitational mysteries. To a large degree of precision, $F_g = \frac{GMm}{r^2}$ describes the motion of objects in the universe, but it fails to account for several large-scale phenomena, like gravitational redshifting or the precession of the perihelion of Mercury.

Newtonian gravity predicts a curvature of

$$\delta_{Newtonian} = \frac{2GM}{c^2 R} \tag{1}$$

in the path of light passing at radius R by a mass M, but general relativity predicts a curvature of

$$\delta_{GR} = \frac{4GM}{c^2 R} = 2\delta_{Newtonian}. \quad [1] \tag{2}$$

In 1919, Arthur Eddington and his team measured the difference in the apparent position of light from stars during a solar eclipse and 6 months earlier, when its path was not affected by the Sun's gravitational pull. They found that the magnitude of the gravitational lensing agreed with Einstein's theory instead of Newtonian gravity. This was the first definitive proof of Einstein's theory, which further experiments would corroborate. [2]

In 1937, Fritz Zwicky suggested that distant dark matter distributions could create gravitational lensing effects across fields of galaxies, and he was eventually proven right. [3] In general relativity, light will bend to follow the geodesic path around massive objects.

As Zwicky suspected, dark matter clumps are scattered throughout the universe in the spaces between luminous galaxies. As light from the background galaxies passes the dark and luminous matter, its path is bent by gravitational lensing. When this light is detected on Earth, the distant galaxies appear slightly squashed or stretched in one direction, just as though they were viewed through an optical lens.

This slight distortion is referred to as the shear. If the shear of a specific galaxy can be measured, the mass distribution between that galaxy and Earth can be measured. Extended matter distributions can distort whole fields of galaxies in a given direction. If the shear of distant galaxy fields can be measured, the intervening mass distribution can be measured, which gives insight into how luminous and dark matter clustered in the early Universe, and how those clusters evolved over time.

This idea is simple in theory, but nearly impossible in practice. Firstly, galaxies are not inherently spherical. Ellipticals are oblate spheroids, and can have a wide range of axis

ratios. Spirals have fairly circular disks, but the flatness of the disk combined with their random orientation often makes them appear quite elliptical when imaged. Even without the deformations caused by galaxy collisions, there is a huge variance in the shape of normal galaxies. Moreover, the random distribution and orientation of galaxies further complicates the problem. The effects of gravitational lensing or tidal forces are indistinguishable from the inherent shape of the galaxy. Also, gravitational shear distortions caused by weak lensing are tiny compared to the intrinsic shape of the galaxies - of order a few percent. [4]

Because it is impossible to measure the shear of an individual galaxy, the shear across a field of galaxies is measured. Algorithms that measure these shears work by assuming that galaxies are 'pointed' in random directions. If the average galaxy directionality is nonzero in a given direction, that is assumed to be the result of gravitational lensing.

These algorithms are effective, but extremely difficult to test. There is no way to know the actual shear for a given galaxy field, so there is no way test the efficacy of the algorithms with real data. To circumvent this problem, artificial test data is generated. Real galaxy images are sheared by a known amount, and then run through the detection algorithms. The output of the detection algorithms can then be compared to the stretching parameters, and the error of the detections can be properly evaluated.

When generating simulated LSST images, the galaxies are sheared and then put into PhoSim, which takes in an image of the galaxy in each filter with its associated spectrum. From this, it generates fake LSST images, with realistic atmospheric distortions. Most projects only handle galaxy images in one filter, which produces monochromatic output. To make full-color sheared images, the original image is separated into different filters and sheared separately. The sheared images are put into PhoSim with an associated spectrum to produce fake LSST images. Each image is separately processed, and the results are added back together to produce the full sheared image. [5]

This approach has worked well in the past, but most multi-color algorithms assume that galaxies have equal flux in all filters. For an n-filter fit, the full-color intensity at each pixel is divided by n. This makes the galaxies appear identical in different filters, which fails to account for internal color variations caused by galaxy structure. Therefore, this method of generating simulated lensing provides less-than-optimal simulations.

This project hope to establish protocols that utilize the existing distortion algorithms, so the output must be of images and assorted spectra. The flat spectrum issue is addressed by decomposing galaxy images into two components, each with a specific associated spectrum. The work rests on the assumption that any galaxy can be represented as a linear combination of the fluxes of two orthogonal spectra. For most of this project, the spectra of the 'typical' spiral and 'typical' elliptical galaxies were used. This assumption works because spiral and elliptical galaxies are different colors overall, so their spectra are markedly different. This project will focus on 'classical' spiral and elliptical galaxies, and ignore edge cases like irregular galaxies. This is because the emphasis is on the differences in spectra are important to the project, and not the structure of the galaxies that produce the model spectra.

In general, elliptical galaxies are older, redder, and more massive than spirals. Spirals are generally modeled as an exponential disk plus an elliptical bulge. The bulge has the same radial profile as elliptical galaxies, and tends to be redder and older than the disk. The disk is bluer, and modeled with an exponential profile.

These color differences are caused by variation in the type of constituent stars. The rate of fusion in the core of a star is determined by the internal temperature and pressure of the star, which is set by a star's radius and mass. Therefore, larger stars will burn hotter and run out of fuel faster than their smaller counterparts. This extra energy output results in more flux at higher wavelengths, which makes larger stars appear bluer than small, red

stars. [6]

In these galaxies, the blue areas correspond to star-forming areas. Stars of all sizes form in these regions, but the new blue stars are replaced as they burn out. In the redder non-star-forming regions, the large blue stars burned out long ago, but no new stars have formed to replace them. The gravitational forces in the spiral arms drives star formation, making the arms bluer than the bulge, where the large blue stars burned out millennia ago. In elliptical galaxies, there is less interstellar gas and dust, and virtually no star formation. [7]

The differences in color and structure make the typical spectra for spirals and ellipticals are very different. When generating the models of galaxies, each model spectra can be used as a sort of eigenvector. Just like a point on a plane could be represented by any two orthogonal axes, any two markedly different spectra could be used to model a galaxy image. Ellipticals and spirals were chosen as a natural starting place, but this project could (and should) be generalized to include other spectra.

3. Methods

In broad terms, the pipeline is as follows:

- Identify model spectra.
- Identify test galaxy images with known redshifts
- Fit the test galaxies as a linear combination of the model spectra.

3.1. Model Spectra

The first step in the process was finding the median flux densities in each filter for spirals and ellipticals. This data was not immediately available for HST data, but could be assembled from existing data sets.

The Cosmic Assembly Near-IR Deep Extragalactic Legacy Survey (CANDELS) project is "designed to document the first third of galactic evolution from z = 8 to 1.5 via deep imaging of more than 250,000 galaxies with WFC3/IR and ACS". [8][9][10] For this project, their spectral catalogs were used. CANDELS has published the flux densities of 7634 HST galaxies in a variety of filters, and lists their RA and DEC.[11][12] Overall, 5520 galaxies have usable flux densities in the chosen filters.

The galaxy classifications were pulled from the CANDELS Visual Classification Project. In this project, 65 human classifiers sorted 12702 galaxies as spirals, ellipticals, irregular, compact, or unresolvable. [13] For this project, the GOODS-S fractional visual classification catalog was used, and the data set can be downloaded from http://cdsarc.u-strasbg.fr/viz-bin/Cat?cat=J%2FApJS%2F221%2F11 &target=readme&#sRM2.2. In the fractional catalogs, galaxies were provided with their RA and DEC, as well as the percentage of users that classified the galaxy as each type. For the purposes of this project, galaxy classifications were discarded if the difference between the two largest fractional

classification categories was ≤ 0.3.

After cleaning both data sets, galaxies were matched by RA and DEC. A galaxy was considered matched if the RA and DEC differences between the catalogs was ≤ 0.0001. The total combined catalog contained 2037 galaxies.

From the compiled data set, the median flux densities of spiral and elliptical galaxies were identified in each filter. These median flux densities were then fed into the fitting algorithm as a measure of the 'typical' fluxes of spiral and elliptical galaxies.

As further discussed in the results section, preliminary error measurement suggested that some redshift-dependent error was introduced. Therefore, redshifted model spectra were used instead of the typical spiral and elliptical fluxes.

3.1.1. Redshifted Model Spectra

Because the universe is expanding, the space between distant galaxies and our telescopes stretches as light travels toward us. The light traveling through that space is stretched as well - which increases its wavelength and makes the light appear redder. For light emitted at redshift z, the emitted frequency ν_e is related to the observed frequency ν_0 via

$$\nu_e = [1 + z]\nu_0 \quad [14] \tag{3}$$

This result is known as cosmological redshift. Distant galaxies with higher redshifts, have more flux toward the redder end of their spectrum, and their initial flux is spread out over a wider area. This effect is difficult to quantify with the data used in this project, so additional information was needed.

In cases like these, k-corrections are usually implemented to accurately redshift the

apparent magnitude of the galaxies in a specific emitted bandpass Q.

$$m_R = M_Q + DM + K_{QR} \tag{4}$$

In this equation, m_R is the apparent magnitude of a galaxy, M_Q is the absolute magnitude, DM is the distance modulus $DM = 5log_{10}\left[\frac{D_L}{10\ pc}\right]$ and K_{QR} is the k-correction, which is a function of the integral of the flux at each wavelength. [14] However, implementing k-corrections requires knowledge of the full emitted spectra of the galaxies, and this project only uses the flux at specific wavelengths. Therefore, k-corrections were impossible for this project. Instead, the fluxes of individual similar-redshift galaxies were used as proxies. This method has the benefit of encoding spectral information about galaxy age in the model spectra, as the younger test galaxies are paired with younger model spectra.

A table of 101 galaxies (Figure 1) with measured redshifts and magnitudes in the appropriate filters was found in Rutkowski et al 2012. [15] When the magnitudes are converted to fluxes are normalized and graphed, a bimodal distribution emerges. The spectra of the galaxies in these two group are assumed to be different enough to serve as new orthogonal model spectra. For each of the test galaxies, the five galaxies in the table with the closest redshift were identified. The spectra of two galaxies - one from each group - were chosen to as new model spectra for the fitting algorithm. However, this data set does not contain fluxes for the F105W filters, so the result of a linear interpolation between the F125W (9166 Å) and F850LP (12459Å) filters was used in its place.

3.2. Data Cleaning

Throughout this project, all values are handed in F_λ, which has units of $\frac{erg}{scm^2\mathring{A}}$. In the CANDELS data set, the flux density is provided in μJy, which is in units of $10^{-6}F_\nu$, which

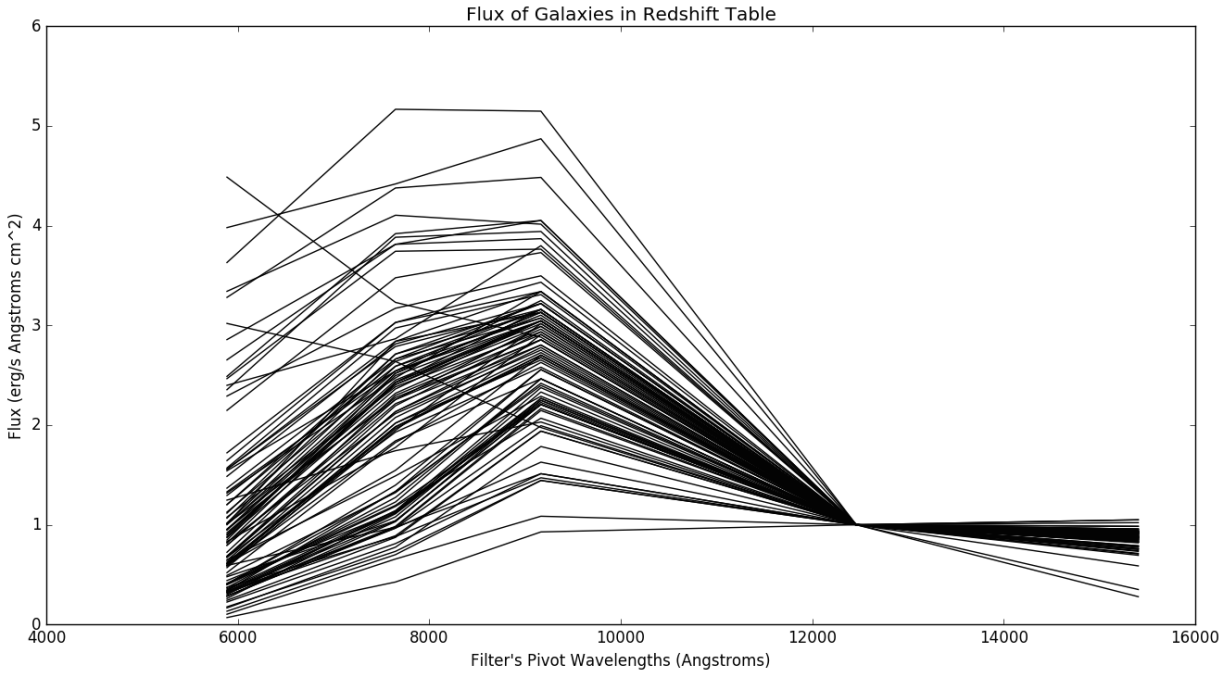

Fig. 1.— Normalized fluxes in the galaxy redshift database. Note the bimodal distribution that emerges in the 6000Å to 8000Å region.

is in $\frac{erg}{scm^2Hz}$. Throughout the project, all values were converted into F_λ. For F_ν,

$$F_\lambda = \frac{c}{\lambda^2} F_\nu \quad [16] \tag{5}$$

In the catalog of redshifted galaxies, the magnitudes were converted into fluxes via

$$F_{lambda} = count\ rate\ \cdot\ PHOTFLAM = PHOTFLAM \cdot 10^{\frac{-(mag-zpt)}{2.5}} \quad [17] \tag{6}$$

The zeropoint magnitudes were from the paper associated with the data [15], and PHOTFLAM measurements were from an STSCI resource on WFC3 zeropoints. [18]

3.3. Test Galaxies

The fitting algorithm was run on galaxies in the F105W, F125W, and F160W filters. HST images and the wide near IR filters were used because the resolution of the images made the size of the galaxies in the images large enough to be fit by the algorithm. So that redshift-induced errors could be accounted for, the test galaxies were pulled from the VUDS-ECDFS-DR1 catalog, which lists galaxies with their RA, DEC, and photometric redshifts. [19][20]

VUDS provides redshift reliability flags (z_{flag}) for each galaxy, and galaxies with $z_{flag} < 3$ were discarded. This only left behind galaxies that have ¿ 95% reliability in their redshift. In their words, this corresponds to at least "moderate to high S/N with several absorption and/or emission lines" and "strong cross-correlation signal with excellent continuum match to templates." [20]

The galaxies in the reliable-redshift catalog were then sorted by apparent magnitude to obtain a list of visible galaxies in the chosen IR filters.

The images were found by searching by RA and DEC in the STSCI database. If the target galaxy was visible in all three filters and the preview images looked satisfactory, the drizzled FITS files were downloaded.

In almost all cases, the F105W filter image needed to be rotated to match the F125W and F160W images. Image rotation measurement was done by eye, and the FITS files were Scipy's ndimage interpolation.rotate function. [21] Once the images had the same orientation, DS9's RA/DEC overlays were used to manually locate the galaxy centers on each image, and the images and galaxy locations were fed into the fitting algorithm. [22]

3.4. Best Fit Algorithm

Once the elliptical and spiral spectra and test galaxy images had been identified, postage stamps were made for each galaxy. Using astropy.io, the input images were cropped to create square images 21 pixels wide centered on the chosen galaxy. [23][24] A Python script was written to find the average background count rate in an empty patch of sky for each image. This background flux was subtracted from each pixel before the fitting algorithm.

The algorithm iterates through the 21x21 array of pixels. For each pixel location, the flux density in each filter is modeled using Scipy's optimization package's curve_fit function. [21] In mathematical terms, the function found values for α and β for each pixel to best fit the following, where $F105W_{sp}$ is the median flux of spiral galaxies in the F105W, etc.

$$F105_{actual}(x, y) = \alpha F105W_{sp} + \beta F105W_{ellip} \tag{7}$$

$$F125_{actual}(x, y) = \alpha F125W_{sp} + \beta F125W_{ellip} \tag{8}$$

$$F160_{actual}(x, y) = \alpha F160W_{sp} + \beta F160W_{ellip} \tag{9}$$

Each pixel has the same values of α and β for the three fitting equations, but they vary from pixel to pixel. α and β are constrained in the curve_fit function to be ≥ 0 . If galaxies are modeled as a linear combination of model spectra, it defies the model to have a galaxy made up of a negative spiral image, for example.

In less mathematical terms: If each pixel in the original image can be written as a linear combination of a typical elliptical and spiral galaxy, it can be further broken down by filter. That is, the flux of the original galaxy in a filter = α (median spiral flux density in that filter) + β (median elliptical flux density in that filter). Each pixel is fit independently,

but the fluxes for an individual pixel are fit with the same values of alpha and beta. The algorithm returns 21x21 arrays of α and β for each galaxy fit.

3.5. Image Data Conversion

In the HST drizzled FITS files, the pixel values are given in count rates - that is, $\frac{e^-}{s}$. To convert these values to F_λ, the PHOTFLAM header value is used. PHOTFLAM is the inverse sensitivity of an exposure, and is given in units of $\frac{erg}{cm^2 sA^\circ}$.

$$F_\lambda = PHOTFLAM \cdot count\ rate \quad [25] \tag{10}$$

Because the pixel values and median fluxes are of order 10^{-20}, they are too close to 0 to be reliably fit by the curve_fit algorithm. To fix this, the fitting equations were scaled up as follows:

$$F105_{actual} \cdot 10^{25} = \alpha \cdot F105_{spiral} \cdot 10^{25} + \beta \cdot F105_{elliptical} \cdot 10^{25} \tag{11}$$

This does not affect the α and β values, but allows Scipy to accurately fit the equations.

This algorithm passed several basic tests, such as returning α=β for flat spectra, and being independent of parameter order for α and β.

The α and β arrays can be used to recreate the galaxy images via

$$F105_{recreation}(x, y) = \alpha F105W_{spiral} + \beta F105W_{elliptical} \tag{12}$$

These recreations are used to test the modeling algorithm and create shearing algorithm input.

4. Results

The code was tested on 5 galaxies with redshifts ranging from z = 0.5481 to z = 1.0467. After the α and β values for each pixel were measured, the original images were recreated. For each pixel, predicted flux density was

$$F105_{recreation}(x,y) = \alpha F105W_{spiral} + \beta F105W_{elliptical} \tag{13}$$

$$F125_{recreation}(x,y) = \alpha F125W_{spiral} + \beta F125W_{elliptical} \tag{14}$$

$$F160_{recreation}(x,y) = \alpha F160W_{spiral} + \beta F160W_{elliptical} \tag{15}$$

This way, the predicted and actual images can be visually compared. Also, residual images are created by subtracting the recreated galaxies from the original images.

The galaxy models and residuals are shown in Fig 2.

Parts of the residual image where the pixel values are less than zero indicate that the model was too bright. If the residual values are greater than zero, the model was too dim. As is visible in these images, the original non-redshifted model tends to overestimate the F105W image and underestimate the F125W and F160W images.

The recreated images and residuals are helpful when making a qualitative fit assessment, but it is important to numerically compare the fit across different galaxies. In order to easily quantify the error in the fit for a given filter, a proportional error is defined for each filter at each pixel such that

$$proportional\ error = \frac{predicted\ flux\ density}{actual\ flux\ density}. \tag{16}$$

Therefore, the ideal galaxy would have values around 1.0 for each pixel. The strange

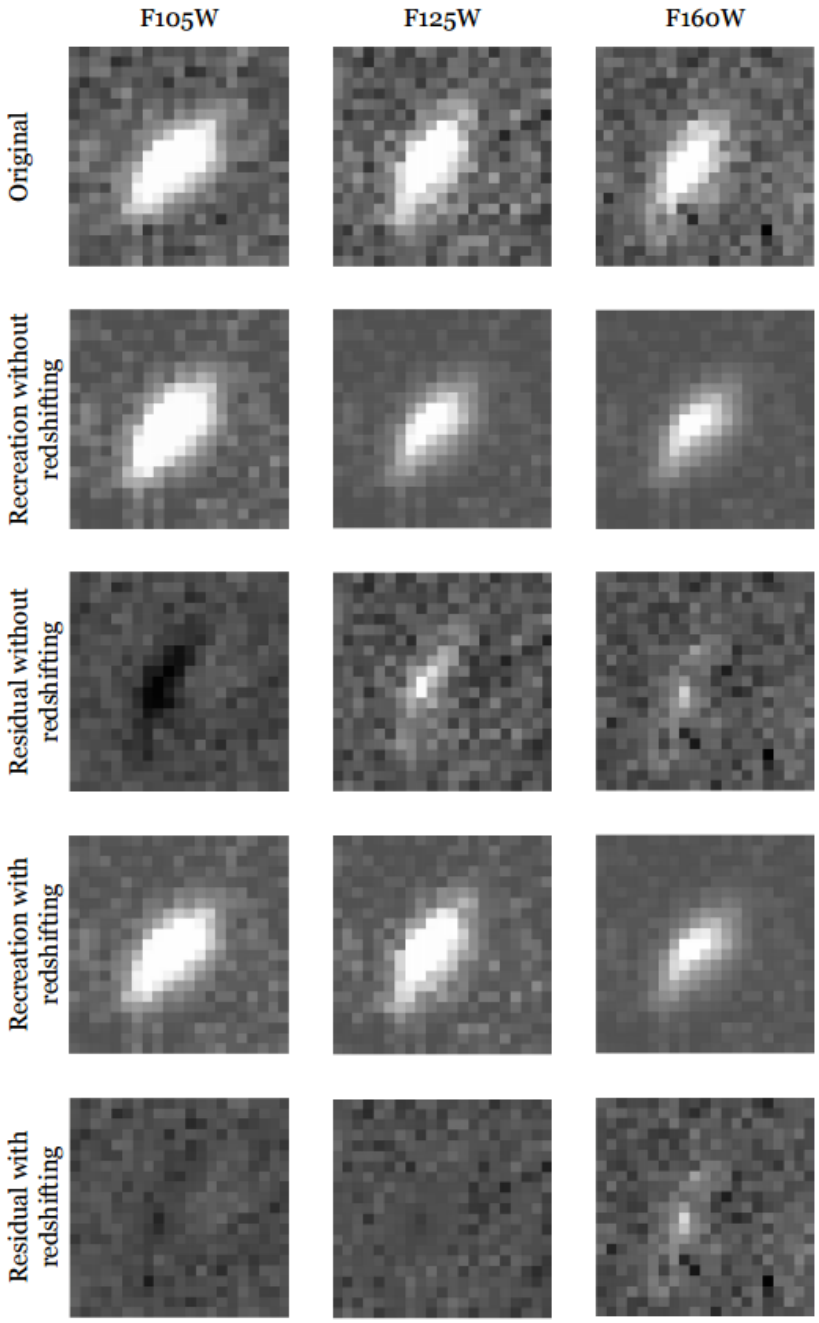

Fig. 2.— From left to right, the F105W, F125W, and F160W images. From top to bottom, the original images, modeled images without redshifted spectra, residuals without redshifted spectra, modeled images with redshifted spectra, and residuals with redshifted spectra. The galaxy images are arbitrarily scaled by the same amount to make visual comparison easier, but the zeropoint remains the same.

behavior at higher values of r stem from the fact that the background of the image outside the galaxy goes to zero, so the denominator is very, very small. To find a rough estimate of error as a function of radius, concentric squares of side length 2r around the central pixel are used as proxies for concentric circles of radii r. For each concentric square, the median proportional error is found. This is what is graphed in Figure 3a-c as median proportional error as a function of r.

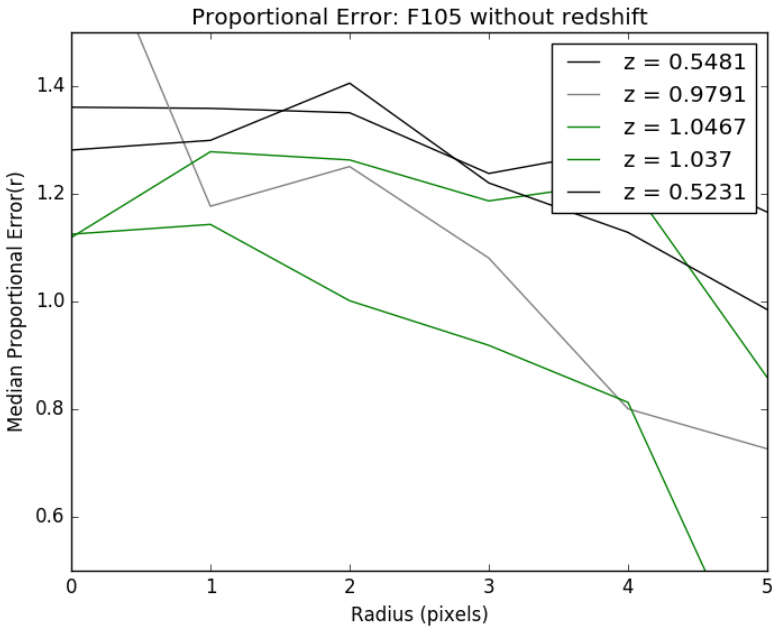

Fig. 3a.— Median error as a function of radius for original spiral and elliptical spectra for the F105W filter.

The results of this project are dependent on the chosen model spectra. If the flux ratios of the chosen model spectra don't match the actual image flux ratios, the fitting algorithm will never produce good results. In the case of the higher-redshift galaxies, a redshift-dependent error is introduced by the spectral mismatch. This effect is evident both in the residual images and graphs, and was the motivation for introducing the redshifted spectra. Encouragingly, the residual images with the redshifted spectra are much better than the original spectra (see Fig 2), and the error graphs similarly improved in Figure 4a-c.

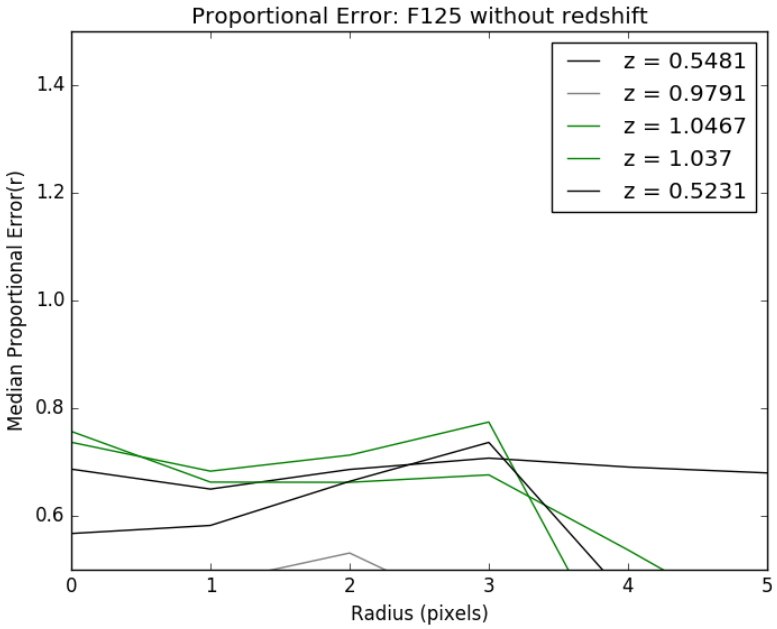

Fig. 3b.— Median error as a function of radius for original spiral and elliptical spectra for the F125W filter.

This suggests that the redshifted model spectra were a step in the right direction.

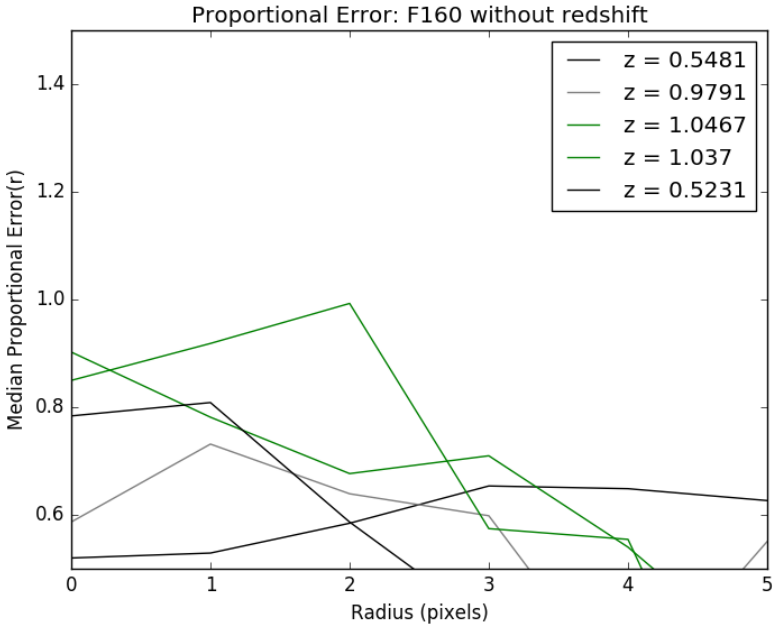

Fig. 3c.— Median error as a function of radius for original spiral and elliptical spectra for the F160W filter.

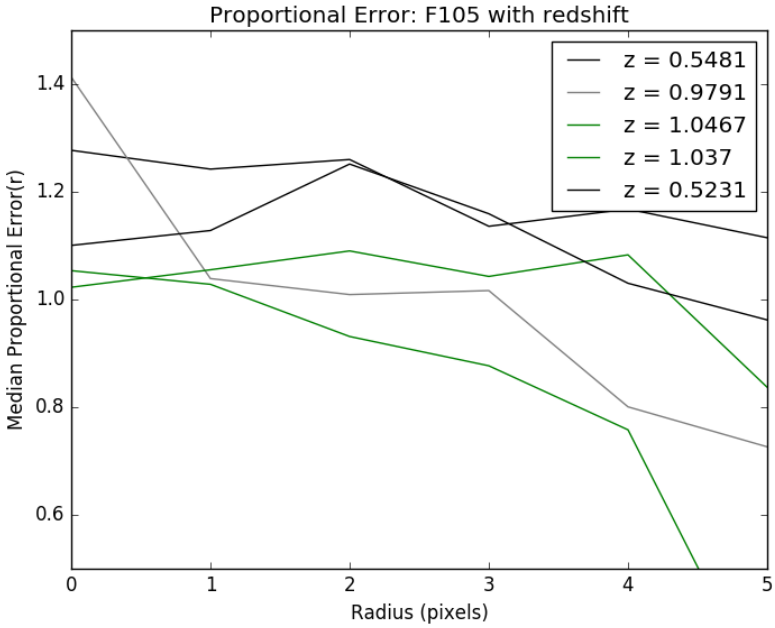

Fig. 4a.— Median error as a function of radius for redshifted spectra for the F105W filter.

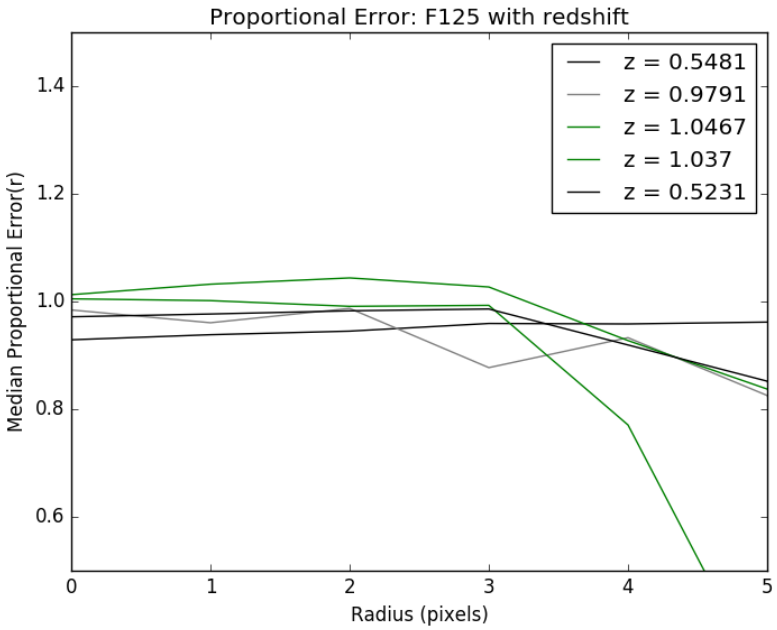

Fig. 4b.— Median error as a function of radius for redshifted spectra for the F125W filter.

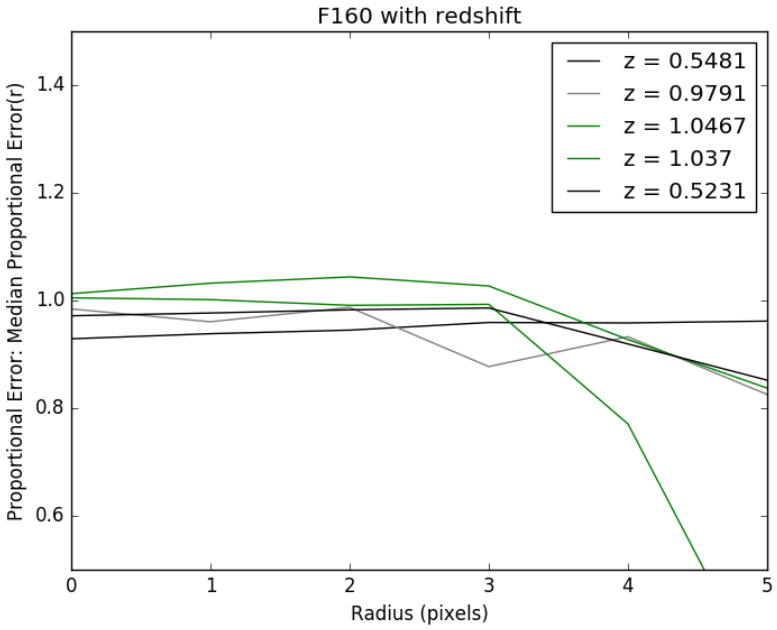

Fig. 4c.— Median error as a function of radius for redshifted spectra for the F160W filter.

5. Limitations and Next Steps

The results of this project are encouraging. With just a two parameter + background fit, the test galaxies can be effectively modeled. However, the fit could be drastically improved by including more than two model spectra. Additionally, the redshifted model spectra could be more rigorously determined from a large distribution of galaxies. Another possible improvement would be a pixel to pixel model to test relationship, instead of whole galaxy to pixel. Basically, the galaxy size would be normalized, and the flux at each test pixel would be a linear combination of the flux at that pixel in the model galaxies. Still, this project was a great success overall.

6. Acknowledgements

Thank you to Professor Dell'antonio for being a fantastic advisor and mentor during this process. Thanks to the Brown Physics Department, friends and family.

7. Software

This project made use of the following programs:

Numpy: Stéfan van der Walt, S. Chris Colbert and Gaël Varoquaux. The NumPy Array: A Structure for Efficient Numerical Computation, Computing in Science & Engineering, 13, 22-30 (2011), DOI:10.1109/MCSE.2011.37 (publisher link)

This work is based on observations taken by the CANDELS Multi-Cycle Treasury Program with the NASA/ESA HST, which is operated by the Association of Universities for Research in Astronomy, Inc., under NASA contract NAS5-26555.

This research made use of Astropy, a community-developed core Python package for Astronomy (Astropy Collaboration, 2013). It also made use of Scipy, specifically the curve-fit function. DS9: Program courtesy of the Smithsonian Astrophysical Observatory at Harvard. Some of the data presented in this paper were obtained from the Mikulski Archive for Space Telescopes (MAST). STScI is operated by the Association of Universities for Research in Astronomy, Inc., under NASA contract NAS5-26555. Support for MAST for non-HST data is provided by the NASA Office of Space Science via grant NNX09AF08G and by other grants and contracts.

8. Citations

1. Soares 2009. Newtonian gravitational deflection of light revisited. http://arxiv.org/pdf/physics/0508030v4.pdf

2. Kutner, Marc L. Astronomy. A Physical Perspective. 2^{nd} Ed. Pg 145.

3. www.amnh.org/education/resources/rfl/web/essaybooks/cosmic/p_zwicky.html

4. Heymans, Van Waerbeke, et al. 2006. STEP 1. http://arxiv.org/pdf/astro-ph/0506112v2.pdf

5. PhoSim. http://www.lsst.org/scientists/simulations/phosim

6. Kutner, Marc L. Astronomy. A Physical Perspective. 2^{nd} Ed. Pg 178.

7. Kutner, Marc L. Astronomy A Physical Perspective. 2^{nd} Ed. Pg 315-319.

8. CANDELS data. http://candels.ucolick.org/data_access/Latest_Release.html

9. CANDELS Survey: Grogin, Kocevski, Faber, et al. 2011. http://arxiv.org/pdf/1105.3753v3.pdf

10. CANDELS HST Data. Koekemoer, Faber, Ferguson et al., 2011. http://iopscience.iop.org/article/10.1088/0067-0049/197/2/36/pdf

11. Flux Data paper. http://candels.ucolick.org/data/public/GOODS-S/ycguo_2013_apjs.pdf

12. Flux data README. https://archive.stsci.edu/pub/hlsp/candels/goods-s/gs-tot/v1.0/hlsp_candels_hst_acs-wfc3_gs-tot_readme_v1.0.pdf

13. Kartaltepe, Mark Mozena, Dale Kocevski et al. 2015. http://arxiv.org/pdf/1401.2455v2.pdf

14. Hogg, Baldry, Blanton, and Eisenstein 2002. http://arxiv.org/pdf/astro-ph/0210394v1.pdf

15. Rutkowski, Cohen, Kaviraj, et al. 2012. http://arxiv.org/pdf/1201.6416v1.pdf

16. http://www.mso.anu.edu.au/pfrancis/ObsTech/BrightnessUnits.pdf

17. Near Infrared Camera and Multi-Object Spectrometer Instrument Handbook for Cycle 17. http://www.stsci.edu/hst/nicmos/documents/handbooks/current_NEW /Appendix_B.14.3.html

18. Zeropoints. http://www.stsci.edu/hst/wfc3/phot_zp_lbn

19. VUDS Redshift Site: http://cesam.lam.fr/vuds/DR1/

20. Tasca, Le F‘evre, Ribeiro, et al. 2016. http://arxiv.org/pdf/1602.01842v1.pdf

21. Jones E, Oliphant E, Peterson P, et al. SciPy: Open Source Scientific Tools for Python, 2001-, http://www.scipy.org/

22. DS9. http://ds9.si.edu/site/Home.html

23. Astropy paper; http://arxiv.org/pdf/1307.6212v1.pdf

24. Astropy: http://dx.doi.org/10.1051/0004-6361/201322068

25. Introduction to the HST Data Handbooks. http://www.stsci.edu/hst/HST_overview/documents/datahandbook/intro_ch35.html